

MIXED FORMULATION OF BOND-SLIP PROBLEMS UNDER CYCLIC LOADS

By Ashraf Ayoub,¹ Student Member, ASCE, and Filip C. Filippou,² Member, ASCE

ABSTRACT: The stress transfer mechanism between reinforcing steel and surrounding concrete through bond and the resulting slip plays an important role in the hysteretic behavior of reinforced concrete structures. Earlier models of the stress transfer problem were based on a displacement formulation. Recent models, however, have demonstrated the significant advantages of a flexibility formulation on account of its accuracy and numerical stability under large inelastic strains in the reinforcing steel and bond damage in the surrounding concrete. This paper presents a critical evaluation of existing anchored reinforcing bar models and proposes a new model based on a two-field mixed formulation in which independent interpolation functions are used for the relative slip and the reinforcing steel forces. The advantages of this approach over existing models are assessed by numerical studies of anchored reinforcing bars under monotonic loads. The accuracy of the proposed model is established by correlation of analytical results with experimental data of an anchored reinforcing bar under severe cyclic loading.

INTRODUCTION

The development of the finite-element method as a powerful and general method of analysis and the ever increasing speed of computer hardware make the nonlinear analysis of even complex concrete structures under seismic loads feasible. The interaction between reinforcing steel and surrounding concrete through bond-slip plays an important role in the hysteretic behavior of these structures. However, the complexity of accurately simulating the stress transfer between steel and concrete in a finite-element model of the structure under cyclic excitations has constrained researchers to assume perfect bond conditions in their studies. This limits the failure prediction capability of the model under monotonic and cyclic loads. To overcome this limitation several studies have been devoted to the modeling of bond between steel and concrete and the resulting slip of the reinforcing bar. While the early studies were limited to monotonic loads, more recent studies have proposed solutions of the problem under large inelastic deformation reversals.

The first proposal for modeling the relative slip between reinforcing bar and concrete dates back to the work of Ngo and Scordelis (1967), who inserted a bond spring or bond link element between reinforcing steel and concrete finite elements. In this pioneering work the bond-slip relation is assumed to be linear elastic. A few years later Nilson (1971) introduced a nonlinear bond-slip relation in the same analysis framework. Refinements of this concept were reported by an ASCE task committee (ASCE 1982).

Because of the limitations of the bond link element, de Groot et al. (1981) proposed a bond-zone element of finite thickness with distributed bond action. In a later study Keuser and Mehlhorn (1987) showed that concentrated bond link elements correctly represent only uniform slip distributions. With this conclusion they introduced a contact element that provides continuous interaction between reinforcing steel and concrete. The behavior of concrete was modified in the vicinity of the contact surface between steel and concrete to account

for the properties of the bond zone. Yankelevsky (1985) proposed a finite-element solution for an anchored reinforcing bar with a piecewise linear bond stress-slip relation. The study is, however, limited to linear elastic behavior of reinforcing steel and accounts only for monotonic loads.

The first analytical models of the hysteretic behavior of anchored reinforcing bars under cyclic loads appeared in the early 1980s (Tassios and Yannopoulos 1981; Ciampi et al. 1982; Filippou et al. 1983b). While the proposed models correlate well with experimental evidence, they are based on classical solution strategies, so that they cannot be readily included in a general-purpose finite-element analysis program. The study by Filippou et al. (1983a) is the first to propose a weighted residual method for solving the differential equations of equilibrium and compatibility of an anchored reinforcing bar. This approach gives rise to a mixed finite-element with independent approximations of the displacement and stress fields in the bar. The formulation, however, was not cast in a finite-element framework and cannot be included in a general-purpose finite-element analysis program. Subsequent studies (Filippou 1986; Zulfiqar and Filippou 1990) reveal the advantages of approximating the smooth steel stress distribution along the anchored reinforcing bar, rather than the relative slip that changes dramatically in the inelastic zone under large strains. This realization, along with the proposal of a consistent implementation of a flexibility-based nonlinear beam element (Ciampi and Carlesimo 1986), led to the formulation of a flexibility-based anchored reinforcing bar element (Monti et al. 1993, 1997). The element proved numerically robust and accurate, but suffers from an ad hoc assumption for the bond stress distribution that leads to a nonsymmetric stiffness matrix for the anchored reinforcing bar. This is an unnecessary penalty in the computer implementation of the element. To overcome this limitation a mixed formulation is proposed in this paper that is based on the independent interpolation of force and displacement fields of the anchored reinforcing bar within the context of a mixed variational principle.

In the following the salient features of the existing models are reviewed. After the mixed formulation of an anchored reinforcing bar is presented, its results are compared against those of the other models in several numerical simulations. These simulations reveal the limitations of existing models and the advantages of the mixed formulation. Finally, the study concludes with the correlation of analytical results with experimental data from the hysteretic behavior of an anchored reinforcing bar under cycles of several slip reversals.

¹Res. Asst., Dept. of Civ. and Envir. Engrg., Univ. of California, Berkeley, CA 94720.

²Prof., Dept. of Civ. and Envir. Engrg., Univ. of California, Berkeley, CA.

Note. Associate Editor: David J. Stevens. Discussion open until November 1, 1999. To extend the closing date one month, a written request must be filed with the ASCE Manager of Journals. The manuscript for this paper was submitted for review and possible publication on August 28, 1998. This paper is part of the *Journal of Structural Engineering*, Vol. 125, No. 6, June, 1999. ©ASCE, ISSN 0733-9445/99/0006-0661-0671/\$8.00 + \$.50 per page. Paper No. 19136.

GOVERNING EQUATIONS OF ANCHORED BAR PROBLEM

The behavior of a reinforcing bar anchored in concrete is governed by four unknown fields: the steel stress $\sigma = \sigma(x)$ and strain $\epsilon = \epsilon(x)$, the bond stress at the interface between steel and concrete $q = q(x)$, and the relative slip of the bar relative to the surrounding concrete $u = u_s(x) - u_c(x)$. Since concrete deformations are much smaller than steel deformations in the postyield range of response of reinforcing steel, they are not pursued further in this study. Thus, $u_c(x) = 0$ and the relative slip is equal to the steel displacement $u(x) = u_s(x)$.

The governing equations for an anchored reinforcing bar that is suitably isolated from a structural subassembly, as shown in Fig. 1, are as follows:

Equilibrium:

$$\sigma_{,x} = \rho q \quad (1)$$

Compatibility:

$$u_{,x} = \epsilon \quad (2)$$

Steel stress-strain relation:

$$\sigma = \hat{\sigma}(\epsilon) \quad (3)$$

Bond stress-slip relation:

$$q = \hat{q}(u) \quad (4)$$

where $\rho = 4/d$ denotes the ratio of reinforcing bar circumference to area, d being the reinforcing bar diameter. A comma denotes the derivative with respect to x . Appropriate boundary conditions for relative slip and for steel stress accompany the differential equations, e.g., at the beam-column interface in Fig. 1.

In the context of the finite-element solution strategies for (1)–(4) that are compared in this study, the solution domain is divided into discrete elements. On account of the nonlinear character of the material relations in (3) and (4), consistent linearization of the governing equations for a single element is used to derive the incremental force-deformation relation of a single element. The incremental force-displacement relation of the structure is then assembled from the element contributions following well-established principles of structural anal-

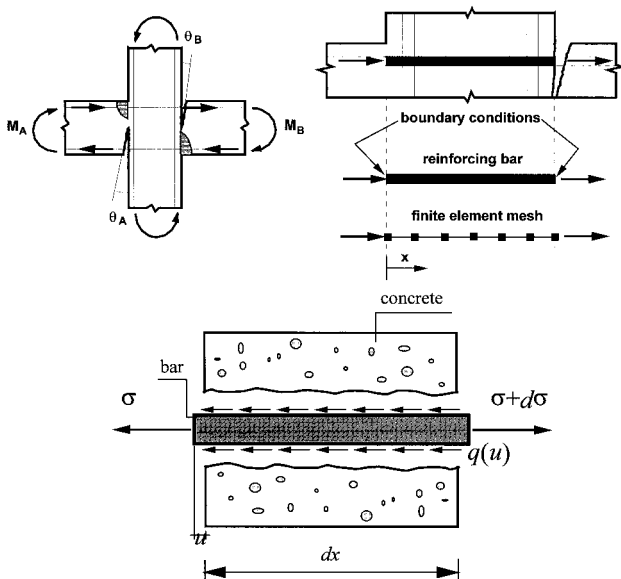


FIG. 1. Anchored Reinforcing Bar Problem in Seismic Analysis: Boundary Conditions and Infinitesimal Segment of Anchored Reinforcing Bar

ysis. The resulting system of equations is solved by an iterative solution strategy, commonly of Newton-Raphson type. In this solution approach, loads or displacements are imposed in several steps on the structure; for each step the linearized system of equations about the current state of the structure is solved for the unknown increments of the primary variables. The current state is updated by determining the structural stiffness and the residual between imposed and resulting forces or displacements, and the process proceeds with the determination of new increments for the primary variables under the residuals. The iteration continues until convergence is achieved to within a specified tolerance, after which the solution algorithm advances to the next load step. The following discussion refers to a single Newton-Raphson iteration, denoted by superscript i , within a load step of the incremental solution strategy for the governing nonlinear equations.

Displacement Formulation

In the displacement formulation the nodal displacements serve as primary variables. The cornerstone of the displacement formulation within a finite-element context is the weighted integral form of the equilibrium equation. The formulation follows these steps:

1. The displacement field of a typical element is approximated with a suitable function $\mathbf{a}(x)$:

$$u(x) = \mathbf{a}(x)\mathbf{u} \quad (5)$$

where $u(x)$ represents the relative slip of the reinforcing bar at point x ; $\mathbf{a}(x)$ is the row vector of n_d displacement interpolation functions; and \mathbf{u} is the vector of n_d nodal displacements.

2. The equilibrium equation at the current state of the element is cast in weighted integral form by invoking the principle of virtual displacements:

$$\int_0^L \delta u^T(x) [\sigma_{,x}^i(x) - \rho q^i(x)] dx = 0 \quad (6)$$

where $\delta u(x)$ are the virtual displacements in the role of a weight function. The integration by parts of the first term in the integral yields

$$\delta u^T(x) \sigma^i(x) \Big|_0^L - \int_0^L \delta u_{,x}^T(x) \sigma^i(x) dx - \int_0^L \delta u^T(x) \rho q^i(x) dx = 0 \quad (7)$$

The consistent linearization of the nonlinear bond stress-slip relation $q^i(x) = q^{i-1}(x) + k_b^{i-1}(x) \Delta u^i$ in (7) yields

$$\begin{aligned} \delta u^T(x) \sigma^i(x) \Big|_0^L - \int_0^L \delta u_{,x}^T(x) \sigma^i(x) dx \\ - \int_0^L \delta u^T(x) \rho [q^{i-1}(x) + k_b^{i-1}(x) \Delta u^i(x)] dx = 0 \end{aligned} \quad (8)$$

where q^{i-1} is the bond stress at the end of the last iteration and k_b^{i-1} the corresponding stiffness. The consistent linearization of the nonlinear steel stress-strain relation $\sigma^i(x) = \sigma^{i-1}(x) + k_s^{i-1}(x) \Delta \epsilon^i$ in the first integral of (8) yields

$$\begin{aligned} \delta u^T(x) \sigma^i(x) \Big|_0^L - \int_0^L \delta u_{,x}^T(x) [\sigma^{i-1}(x) + k_s^{i-1}(x) \Delta \epsilon^i(x)] dx \\ - \int_0^L \delta u^T(x) \rho [q^{i-1}(x) + k_b^{i-1}(x) \Delta u^i(x)] dx = 0 \end{aligned} \quad (9)$$

where σ^{i-1} is the steel stress at the end of the last iteration and k_s^{i-1} the corresponding stiffness. Eq. (9) represents the weak or integral form of the equilibrium equations of the anchored reinforcing bar problem.

3. The substitution of the displacement approximation from (5) into the weak form and the use of the same interpolation function for the virtual displacements according to Galerkin yields

$$\begin{aligned} \delta \mathbf{u}^T & \left[\int_0^L \mathbf{a}_{xx}^T(x) k_s^{i-1}(x) \mathbf{a}_{xx}(x) dx + \int_0^L \mathbf{a}^T(x) \rho k_b^{i-1}(x) \mathbf{a}(x) dx \right] \Delta \mathbf{u}^i \\ & = \delta \mathbf{u}^T \left[\mathbf{P} - \int_0^L \mathbf{a}_{xx}^T(x) \sigma^{i-1}(x) dx - \int_0^L \mathbf{a}^T(x) \rho q^{i-1} dx \right] \end{aligned} \quad (10)$$

where \mathbf{P} are the applied external forces and $\delta \mathbf{u}$ the virtual displacements at the nodes. On account of the arbitrary nature of $\delta \mathbf{u}$, (10) simplifies to

$$(\mathbf{K}_s^{i-1} + \mathbf{K}_b^{i-1}) \Delta \mathbf{u}^i = \mathbf{P} - \mathbf{Q}_s^{i-1} - \mathbf{Q}_b^{i-1} \quad (11)$$

where $\mathbf{K}_s^{i-1} = \int_0^L \mathbf{a}_{xx}^T(x) k_s^{i-1}(x) \mathbf{a}_{xx}(x) dx$ is the steel contribution to the element stiffness matrix; $\mathbf{K}_b^{i-1} = \int_0^L \mathbf{a}^T(x) \rho k_b^{i-1}(x) \mathbf{a}(x) dx$ is the bond contribution of the element stiffness matrix; $\mathbf{Q}_s^{i-1} = \int_0^L \mathbf{a}_{xx}^T(x) \sigma^{i-1}(x) dx$ is the steel contribution to the resisting forces; and $\mathbf{Q}_b^{i-1} = \int_0^L \mathbf{a}^T(x) \rho q^{i-1} dx$ is the bond contribution to the resisting forces. By respecting the displacement compatibility at the nodes of the finite-element representation of the structure, the equilibrium equations of the entire anchored reinforcing bar can be obtained by direct assembly of the stiffness and resisting force contributions. The primary variables of the resulting system of linear equations are the displacement increments $\Delta \mathbf{u}^i$ at the nodes of the finite-element model. This system of equations is solved for $\Delta \mathbf{u}^i$, after which the state of all elements is updated by determining new stiffness and resisting forces under $\mathbf{u}^i = \mathbf{u}^{i-1} + \Delta \mathbf{u}^i$. Eq. (11) is then resolved for $\Delta \mathbf{u}^{i+1}$ until convergence. The latter is controlled by the ratio of the external work increment in the last iteration to the work increment in the first iteration of the load step. A value of 10^{-12} is used for this ratio in this study.

Because (10) includes first derivatives of the displacement interpolation functions $\mathbf{a}(x)$, these functions need to be continuous at the interelement boundary. The derivative, however, does not have to be continuous. As a result, this formulation does not enforce strain continuity at the element boundary.

Displacement-based models have been used successfully in the simulation of the monotonic load-displacement response of anchored reinforcing bars. Since reinforcing steel strains exhibit abrupt changes in the yielding portion of the bar, particularly under cyclic load reversals, a fine discretization of this portion is indispensable for accuracy and numerical stability. Even with a fine discretization numerical problems are quite common for strength softening conditions under bar pull-out (Viathanatepa et al. 1979). These problems can be overcome by the approximation of the smooth steel stress distribution along the bar instead of the relative slip. The advantages of this approach were pointed out in earlier studies (Bertero et al. 1978; Filippou 1986; Zulfikar and Filippou 1990), but the first consistent implementation within a general-purpose finite-element analysis program is the flexibility formulation by Monti et al. (1993, 1997).

Flexibility Formulation

The flexibility formulation is based on the interpolation of stresses rather than displacements. Monti et al. (1997) use the

bond stresses at the element nodes as primary variables. Because of the relatively smooth variation of bond stresses along an anchored reinforcing bar and the exact satisfaction of equilibrium, excellent results can be obtained with very few elements, even under conditions of strength softening and cyclic load reversal. This is a significant advantage of the flexibility over the displacement formulation, as it reduces the total number of degrees of freedom in the model. The cornerstone of the flexibility formulation is the weighted integral form of the compatibility equation, (2). The formulation follows these steps:

1. The bond stress distribution is approximated with a suitable interpolation function within a typical element:

$$q(x) = \mathbf{b}_b(x) \mathbf{q} \quad (12)$$

where $q(x)$ is the bond stress at point x ; $\mathbf{b}_b(x)$ is a row vector of n_s bond interpolation functions; and \mathbf{q} is the vector of n_s nodal bond stresses.

2. The compatibility equation, (2), at the current element state is cast in weighted integral form by invoking the principle of virtual forces:

$$\int_0^L \delta \sigma^T(x) [u_{xx}^i(x) - \epsilon^i(x)] dx = 0 \quad (13)$$

where $\delta \sigma(x)$ are the virtual stresses in the role of a weight function. The integration by parts of the first term in the integral yields

$$\delta \sigma^T(x) u^i(x) \Big|_0^L - \int_0^L \delta \sigma_{xx}^T(x) u^i(x) dx - \int_0^L \delta \sigma^T(x) \epsilon^i(x) dx = 0 \quad (14)$$

The consistent linearization of the steel stress-strain relation in inverse form $\epsilon^i = f_s^{i-1} \Delta \sigma^i + \epsilon^{i-1}$ in (14) yields

$$\begin{aligned} & \int_0^L \delta \sigma^T(x) [\epsilon^{i-1}(x) + f_s^{i-1}(x) \Delta \sigma^i(x)] dx \\ & + \int_0^L \delta \sigma_{xx}^T(x) u^i(x) dx = \delta \sigma^T(x) u^i(x) \Big|_0^L \end{aligned} \quad (15)$$

The inverse form is necessary here to ensure symmetry (Zienkiewicz and Taylor 1989). The quantity ϵ^{i-1} is the steel strain at the end of the last iteration and f_s^{i-1} the corresponding steel flexibility. The linearization of the bond stress-slip relation in inverse form $u^i = f_b^{i-1} \Delta q^i + u^{i-1}$ in (15) yields

$$\begin{aligned} & \int_0^L \delta \sigma^T(x) [\epsilon^{i-1}(x) + f_s^{i-1}(x) \Delta \sigma^i(x)] dx + \int_0^L \delta \sigma_{xx}^T(x) [u^{i-1}(x) \\ & + f_b^{i-1}(x) \Delta q^i(x)] dx = \delta \sigma^T(x) u^i(x) \Big|_0^L \end{aligned} \quad (16)$$

u^{i-1} being the relative slip at the end of the last iteration and f_b^{i-1} the corresponding bond flexibility. Substituting the equilibrium equation, (1), for the bond stress increments into (16) yields

$$\begin{aligned} & \int_0^L \delta \sigma^T(x) f_s^{i-1}(x) \Delta \sigma^i(x) dx + \int_0^L \delta \sigma_{xx}^T(x) f_b^{i-1}(x) \gamma \Delta \sigma_{xx}^i dx \\ & = \delta \sigma^T(x) u^i(x) \Big|_0^L - \int_0^L \delta \sigma^T(x) \epsilon^{i-1}(x) dx \\ & - \int_0^L \delta \sigma_{xx}^T(x) u^{i-1}(x) dx \end{aligned} \quad (17)$$

where $\gamma = 1/\rho = d/4$. Eq. (17) represents the weak or integral form of the compatibility equation and is the counterpart of (9).

3. The substitution of the bond stress approximation from (12) into the weak form yields after several transformations (Monti et al. 1997)

$$[\mathbf{K}_s^{i-1} + \mathbf{K}_b^{i-1}]\Delta \mathbf{u}^i = \mathbf{P} - \mathbf{Q}_s^{i-1} - \mathbf{Q}_b^{i-1} \quad (18)$$

with the following definitions:

$$\mathbf{K}_s^{i-1} = k_s^{i-1} \begin{bmatrix} 1 & -1 \\ -1 & 1 \end{bmatrix}$$

is the steel stiffness matrix with

$$k_s^{i-1} = \left[\int_0^L f_s^{i-1}(x) dx \right]^{-1}$$

and

$$\mathbf{K}_b^{i-1} = \rho \frac{L}{2} \left\{ \begin{bmatrix} -N_{qI} \\ N_{qJ} \end{bmatrix} - k_s^{i-1} \begin{bmatrix} -\mathbf{N}_Q^{i-1} \\ \mathbf{N}_Q^{i-1} \end{bmatrix} \right\} \mathbf{E}_q^{i-1}$$

is the bond stiffness matrix. The quantities

$$\mathbf{N}_q(\xi) = \left[-\frac{1}{4}(1-\xi)^2 + \frac{1}{2} \frac{1}{4}(1+\xi)^2 - \frac{1}{2} \right]$$

are stress interpolation functions with $\xi = (2x/L) - 1$. $I(\xi = -1)$ and $J(\xi = 1)$ denote the left and right element nodes, respectively. Next,

$$\mathbf{N}_Q^{i-1} = \int_0^L f_s^{i-1}(x) \mathbf{N}_q(x) dx$$

$$\mathbf{E}_q^{i-1} = \begin{bmatrix} k_{bI}^{i-1} & 0 \\ 0 & k_{bJ}^{i-1} \end{bmatrix}$$

with k_b the bond stiffness at the corresponding end node, and

$$\mathbf{Q}_s^{i-1} = \frac{1}{2} \begin{bmatrix} 1 & -1 \\ -1 & 1 \end{bmatrix} \mathbf{S}_s^{i-1}$$

is the steel contribution to the resisting forces, where \mathbf{S}_s^{i-1} is the steel force at the element ends. Finally,

$$\mathbf{Q}_b^{i-1} = \rho \frac{L}{2} \begin{bmatrix} -N_{qI} \\ N_{qJ} \end{bmatrix} \mathbf{q}^{i-1}$$

is the bond contribution to the element resisting forces, where

$$\mathbf{q}^{i-1} = \begin{bmatrix} q_{bI}^{i-1} \\ q_{bJ}^{i-1} \end{bmatrix}$$

and q_{bI} , q_{bJ} are the bond resisting forces at ends I and J , respectively.

The numerical implementation of the flexibility formulation by Monti et al. (1997) resulted in an element iteration to satisfy the compatibility requirement on the right-hand side of (17). While this internal iteration increases the computational effort of the element state determination process, the smaller number of elements in an anchored bar model results in a reduction of the number of model degrees of freedom and more than compensates for the additional computational effort. Moreover, the model is numerically very robust even in the presence of the significant strength softening associated with pull-out of the reinforcing bar. But the model has some shortcomings:

1. The bond stress-slip relation is only invoked at the element nodes; this works against the major advantage of

the flexibility formulation of increasing solution accuracy by increasing the number of integration points without necessarily refining the finite-element discretization of the model (Neuenhofer and Filippou 1997).

2. The weight function $\delta\sigma(x)$ is assumed constant within the element, so as to eliminate the contribution of relative slip in the second term of the left-hand side of (15), while the steel stress distribution is assumed to be parabolic; this deviation from a Galerkin solution results in a non-symmetric stiffness matrix, thus, increasing storage demands and computational effort.
3. Finally, no information is available about the relative slip distribution in the element, since the formulation only makes use of the slip values at the nodes.

These problems arise from the basic fact that it is not possible to satisfy exactly the equilibrium equations of the problem by appropriate selection of stress interpolation functions, as is the case in the flexibility formulation of beam elements with linear geometry (Neuenhofer and Filippou 1997). Consequently, a pure flexibility formulation hinges on several ad hoc assumptions that give rise to the aforementioned limitations (Monti et al. 1993, 1997). These limitations of a pure flexibility formulation are the motivation for the more general solution approach in this paper, which makes use of independent interpolation of internal forces and of relative slip in the anchored reinforcing bar element. This leads to a mixed or hybrid formulation that overcomes the limitations of the flexibility formulation and results in an element that combines the efficiency and numerical robustness of the flexibility method with the accurate representation of relative slip in the displacement method.

Two-Field Mixed Formulation

In the mixed or hybrid formulation of a finite-element solution, the governing equations of the problem are not reduced to a single force or displacement field as in the previous two methods. Instead, two or more independent fields are used, so that several variations are possible (Zienkiewicz and Taylor 1989): $u - \sigma$ field approximation, $u - \varepsilon - \sigma$ field approximation, and $u - \varepsilon - q$ field approximation. For the anchored bar problem, results from pull-out tests show that the steel strains change abruptly over the inelastic portion near the bar ends, while their integral, the relative slip, shows a smoother distribution over the same region. Consequently, it is advantageous from a numerical standpoint to approximate the displacement field rather than the strain field, and the $u - \sigma$ field approximation is used in this study. The $u - \sigma$ mixed formulation is based on the weighted integral form of the equilibrium and compatibility equations and follows these steps:

1. The displacement field of a typical element is approximated with a suitable function $\mathbf{a}(x)$:

$$u(x) = \mathbf{a}(x)\mathbf{u} \quad (19)$$

where $u(x)$ is the displacement at point x ; $\mathbf{a}(x)$ is the row vector of n_d shape functions; and \mathbf{u} is the vector of n_d nodal displacements.

2. The steel stress field of a typical element is approximated with a suitable function $\mathbf{b}(x)$:

$$\sigma(x) = \mathbf{b}(x)\boldsymbol{\sigma} \quad (20)$$

where $\sigma(x)$ is the stress at point x ; $\mathbf{b}(x)$ is the row vector of n_s stress interpolation functions; and $\boldsymbol{\sigma}$ is the vector of n_s nodal stresses. It is worth noting that n_d and n_s do not have to be equal.

3. The first relation of the mixed formulation derives from the weighted integral form of the compatibility equation, (2), at the current element state and takes the form

$$\int_0^L \delta \sigma^T(x) [u_{,xx}^i(x) - \varepsilon^i(x)] dx = 0 \quad (21)$$

where $\delta \sigma(x)$ is the virtual stress field in the role of a weight function and i denotes the global Newton-Raphson iteration number.

The consistent linearization of the steel stress-strain relation in inverse form yields

$$\varepsilon^i = f_s^{i-1} \Delta \sigma^i + \varepsilon^{i-1} \quad (22)$$

where ε^{i-1} is the steel strain at the end of the last iteration and f_s^{i-1} the corresponding steel flexibility. The inverse form of the constitutive relation is necessary here to ensure symmetry (Zienkiewicz and Taylor 1989).

The substitution of (22) into (21) yields

$$\int_0^L \delta \sigma^T(x) [u_{,xx}^i(x) - f_s^{i-1}(x) \Delta \sigma^i(x) - \varepsilon^{i-1}(x)] dx = 0 \quad (23)$$

This is the first of two relations that form the basis of the mixed formulation.

4. With the substitution of the assumed displacement and force interpolation functions from (19) and (20) into (23) and with the use of the same interpolation functions for the corresponding virtual fields according to Galerkin, (23) takes the form

$$\delta \sigma^T \left\{ \left[\int_0^L \mathbf{b}^T(x) \mathbf{a}_{,xx}(x) dx \right] \mathbf{u}^i - \left[\int_0^L \mathbf{b}^T(x) f_s^{i-1}(x) \mathbf{b}(x) dx \right] \Delta \sigma^i - \int_0^L \mathbf{b}^T(x) \varepsilon^{i-1}(x) dx \right\} = 0 \quad (24)$$

Since (24) holds for any $\delta \sigma$, it follows that

$$\left[\int_0^L \mathbf{b}^T(x) \mathbf{a}_{,xx}(x) dx \right] \mathbf{u}^i - \left[\int_0^L \mathbf{b}^T(x) f_s^{i-1}(x) \mathbf{b}(x) dx \right] \Delta \sigma^i - \int_0^L \mathbf{b}^T(x) \varepsilon^{i-1}(x) dx = 0 \quad (25)$$

and after replacing \mathbf{u}^i by $\mathbf{u}^{i-1} + \Delta \mathbf{u}^i$, (25) becomes

$$\mathbf{T} \Delta \mathbf{u}^i - \mathbf{F}_s^{i-1} \Delta \sigma^i - \mathbf{u}_r^{i-1} = 0 \quad (26)$$

with

$$\mathbf{T} = \int_0^L \mathbf{b}^T(x) \mathbf{a}_{,xx}(x) dx$$

$$\mathbf{F}_s^{i-1} = \int_0^L \mathbf{b}^T(x) f_s^{i-1}(x) \mathbf{b}(x) dx$$

$$\mathbf{u}_r^{i-1} = \int_0^L \mathbf{b}^T(x) \varepsilon^{i-1}(x) dx - \mathbf{T} \mathbf{u}^{i-1}$$

\mathbf{F}_s is the steel element flexibility matrix and \mathbf{u}_r^{i-1} is the vector of end displacement residuals at the end of the previous iteration. These residuals represent the compatibility error between end displacements \mathbf{u}^{i-1} and strain distribution $\varepsilon^{i-1}(x)$.

5. The weighted integral form of equilibrium (1) at the current element state takes the form

$$\int_0^L \delta u^T(x) [\sigma_{,xx}^i(x) - \rho q^i(x)] dx = 0 \quad (27)$$

Integrating by parts the first term in the integral yields

$$\delta u^T(x) \sigma^i(x) \Big|_0^L - \int_0^L \delta u_{,xx}^T(x) \sigma^i(x) dx - \int_0^L \delta u^T(x) \rho q^i(x) dx = 0 \quad (28)$$

With the consistent linearization of the bond stress-slip relation $q^i(x) = q^{i-1}(x) + k_b^{i-1}(x) \Delta u^i$, (28) becomes

$$\delta u^T(x) \sigma^i(x) \Big|_0^L - \int_0^L \delta u_{,xx}^T(x) \sigma^i(x) dx - \int_0^L \delta u^T(x) \rho q^{i-1}(x) dx - \int_0^L \delta u^T(x) \rho k_b^{i-1}(x) \Delta u^i(x) dx = 0 \quad (29)$$

Eq. (29) forms, together with (23), the basis of the two field mixed formulation.

6. With the substitution of the assumed displacement and force interpolation functions from (19) and (20) into (29) and with the use of the same interpolation functions for the corresponding virtual fields according to Galerkin, (29) takes the form

$$\delta \mathbf{u}^T \left\{ \left[\int_0^L \mathbf{a}_{,xx}^T(x) \mathbf{b}(x) dx \right] \sigma^i + \left[\int_0^L \mathbf{a}^T(x) \rho k_b^{i-1}(x) \mathbf{a}(x) dx \right] \Delta \mathbf{u}^i \right\} = \delta \mathbf{u}^T \left[\mathbf{a}^T(x) \sigma^i(x) \Big|_0^L - \int_0^L \mathbf{a}^T(x) \rho q^{i-1}(x) dx \right] \quad (30)$$

Since (30) holds for arbitrary $\delta \mathbf{u}$, it follows that

$$\left[\int_0^L \mathbf{a}_{,xx}^T(x) \mathbf{b}(x) dx \right] \sigma^i + \left[\int_0^L \mathbf{a}^T(x) \rho k_b^{i-1}(x) \mathbf{a}(x) dx \right] \Delta \mathbf{u}^i = \mathbf{a}^T(x) \sigma^i(x) \Big|_0^L - \int_0^L \mathbf{a}^T(x) \rho q^{i-1}(x) dx \quad (31)$$

and after replacing σ^i by $\sigma^{i-1} + \Delta \sigma^i$ in the first term on the left-hand side, (31) becomes

$$\left[\int_0^L \mathbf{a}_{,xx}^T(x) \mathbf{b}(x) dx \right] \Delta \sigma^i + \left[\int_0^L \mathbf{a}^T(x) \rho k_b^{i-1}(x) \mathbf{a}(x) dx \right] \Delta \mathbf{u}^i = \mathbf{P} - \left[\int_0^L \mathbf{a}_{,xx}^T(x) \mathbf{b}(x) dx \right] \sigma^{i-1} - \int_0^L \mathbf{a}^T(x) \rho q^{i-1}(x) dx \quad (32)$$

or

$$\mathbf{T}^T \Delta \sigma^i + \mathbf{K}_b^{i-1} \Delta \mathbf{u}^i = \mathbf{P} - \mathbf{T}^T \sigma^{i-1} - \mathbf{Q}_b^{i-1} \quad (33)$$

where

$$\mathbf{K}_b^{i-1} = \int_0^L \mathbf{a}^T(x) \rho k_b^{i-1}(x) \mathbf{a}(x) dx$$

is the bond contribution to the element stiffness

$$\mathbf{Q}_b^{i-1} = \int_0^L \mathbf{a}^T(x) \rho q^{i-1}(x) dx$$

is the bond contribution to the element resisting forces, \mathbf{P} is the vector of applied external loads, and

$$\mathbf{T} = \int_0^L \mathbf{b}^T(x) \mathbf{a}_{,xx}(x) dx$$

as before.

Denoting by \mathbf{Q}_s^{i-1} the steel contribution to the resisting forces $\mathbf{T}^T \boldsymbol{\sigma}^{i-1}$ and combining (26) and (33) into a single matrix relation yields

$$\begin{bmatrix} -\mathbf{F}_s^{i-1} & \mathbf{T} \\ \mathbf{T}^T & \mathbf{K}_b^{i-1} \end{bmatrix} \begin{bmatrix} \Delta \boldsymbol{\sigma}^i \\ \Delta \mathbf{u}^i \end{bmatrix} = \begin{bmatrix} \mathbf{P} - \mathbf{Q}_s^{i-1} - \mathbf{Q}_b^{i-1} \\ \mathbf{0} \end{bmatrix} \quad (34)$$

Eq. (34) represents the matrix form of the compatibility and equilibrium equations of the anchored bar problem in the mixed formulation. On the right-hand side are the displacement residuals \mathbf{u}_r^{i-1} from the violation of the compatibility equation at the end of the last Newton-Raphson iteration, and the unbalanced forces $\mathbf{P} - \mathbf{Q}_s^{i-1} - \mathbf{Q}_b^{i-1}$, which only make sense in the assembled form at the structural level, since \mathbf{P} cannot be isolated for each element. It should be noted that as the iterative solution converges in each load step, the displacement residuals \mathbf{u}_r^{i-1} reduce to 0 in each element, thus satisfying element compatibility. The same is true for the assembled unbalanced forces at the structural level, thus satisfying global equilibrium.

The integrals in the expressions of (34) include first derivatives of the displacement interpolation function $\mathbf{a}(x)$, requiring that this be continuous across element boundaries. By contrast, the stress interpolation function $\mathbf{b}(x)$ can be discontinuous, since no derivatives appear in the integrals of the expressions in (34).

NUMERICAL IMPLEMENTATION OF MIXED FORMULATION

The numerical implementation of the flexibility as well as the mixed formulation is not as straightforward as that of the displacement formulation, when the finite element is part of a general-purpose finite-element analysis program that is based on the direct stiffness method of analysis. Nonetheless, recent studies (Neuenhofer and Filippou 1997) show that the process can be accomplished without an internal element iteration. In this form the element state determination of the flexibility and mixed formulation require only a few additional steps compared with the displacement formulation, but still result in computational savings on account of the smaller number of global degrees of freedom in the structural model for comparable accuracy in global and local response (Neuenhofer and Filippou 1997). An alternative implementation with internal iteration in each element is also possible and can be computationally beneficial in a parallel processing environment, since it shifts some of the computational burden from global (structural) to local (element) iterations. With this in mind, both numerical implementation strategies are briefly described in the following. Furthermore, two options present themselves in the numerical implementation of the mixed formulation: (a) retention of stress degrees of freedom at the structural level or (b) condensation of stress degrees of freedom at the element level and retention of only displacement degrees of freedom at the structural level. These options will be briefly evaluated in the following.

Element State Determination with Independent Stress Degrees of Freedom

In this case the system of equations in (34) is assembled for the entire structure by imposing displacement compatibility and stress continuity at the structural nodes. It is then solved once for each iteration within a step of the incremental solution of the global equilibrium equations. Each node has two unknowns (degrees of freedom): the relative slip and the steel stress. The size of the element matrix is $(n_d + n_s) \times (n_d + n_s)$. It is worth noting that no external actions are present at the stress degree of freedom. The only terms on the right-hand

side of the corresponding equations are the displacement (relative slip) residuals \mathbf{u}_r , which on convergence reduce to 0 and thus satisfy the element compatibility condition. The advantage of this implementation strategy is that it achieves stress continuity at the element boundary by maintaining the stress as an independent global degree of freedom. The additional storage requirement is not significant in a one-dimensional element and is compensated by the accuracy of the steel stress distributions. Another advantage of this strategy is that it does not require an internal element iteration: the element state determination thus works in tandem with the nonlinear iteration strategy at the global degrees of freedom.

Element State Determination with Condensation of Stress Degrees of Freedom

In this option the stress degrees of freedom are condensed out of the system of equations in (34) by solving for $\Delta \boldsymbol{\sigma}$ from the first relation

$$\Delta \boldsymbol{\sigma}^i = (\mathbf{F}_s^{i-1})^{-1} (\mathbf{T} \Delta \mathbf{u}^i - \mathbf{u}_r^{i-1}) \quad (35)$$

The substitution of the stress increment into the second relation of (34) yields

$$\mathbf{T}^T (\mathbf{F}_s^{i-1})^{-1} (\mathbf{T} \Delta \mathbf{u}^i - \mathbf{u}_r^{i-1}) + \mathbf{K}_b^{i-1} \Delta \mathbf{u}^i = \mathbf{P} - \mathbf{Q}_s^{i-1} - \mathbf{Q}_b^{i-1} \quad (36)$$

After collecting terms, (36) becomes

$$[\mathbf{T}^T (\mathbf{F}_s^{i-1})^{-1} \mathbf{T} + \mathbf{K}_b^{i-1}] \Delta \mathbf{u}^i = \mathbf{P} - \mathbf{Q}_s^{i-1} - \mathbf{Q}_b^{i-1} + \mathbf{T}^T (\mathbf{F}_s^{i-1})^{-1} \mathbf{u}_r^{i-1} \quad (37)$$

Eq. (37) is the element equilibrium equation, which can now be assembled for the structural model by imposing displacement compatibility at the nodes. This results in a direct assembly process of element stiffness matrices and resisting force vectors according to well-established principles of matrix structural analysis. The global system of equations is solved iteratively by any one of several possible strategies, of which the classical Newton-Raphson strategy is the best known. During each global iteration an element state determination is required. Two alternative implementations of this state determination are possible:

1. In the iterative element state determination, the internal strain distribution is adjusted until satisfying compatibility in the element and reducing the end displacement residuals \mathbf{u}_r to 0 before returning to the global iteration. In this case (37) becomes

$$[\mathbf{T}^T (\mathbf{F}_s^{i-1})^{-1} \mathbf{T} + \mathbf{K}_b^{i-1}] \Delta \mathbf{u}^i = \mathbf{P} - (\mathbf{Q}_s^{i-1} + \mathbf{Q}_b^{i-1}) \quad (38)$$

with $\mathbf{T}^T (\mathbf{F}_s^{i-1})^{-1} \mathbf{T} + \mathbf{K}_b^{i-1}$ the element stiffness and $\mathbf{Q}_s^{i-1} + \mathbf{Q}_b^{i-1}$ the element resisting forces made up of the steel contribution in the first and the bond contribution in the second term, respectively. The advantage of this formulation over the earlier model by Monti et al. (1993, 1997) is the symmetry of the element stiffness matrix, but more importantly the greater accuracy in the interpolation of relative slip in the element.

2. In the direct element state determination according to the proposal by Neuenhofer and Filippou (1997) the element state determination works in tandem with the solution strategy of the global equilibrium equations, and the end displacement residuals contribute to the element resisting forces according to (37). Upon convergence of the global iterations, these displacement residuals reduce to 0, thus, satisfying compatibility in each element.

While the direct element state determination involves fewer operations inside the element, it often requires an extra itera-

tion in each load step of the incremental solution of the global equilibrium equations relative to the iterative element state determination. Thus, the size of the system of equations to be solved is decisive as to which method is more computationally efficient. For a large number of global degrees of freedom, the extra global iteration of the direct element state determination is more expensive than the element iterations and the first option should be selected. The opposite is true for systems with a small number of degrees of freedom.

The condensation of stress degrees of freedom at the element level results in lack of continuity of the stress field across element boundaries. This discontinuity can, however, be minimized with proper selection of stress and displacement interpolation functions, as discussed in the following section.

Stability of Mixed Formulation

The order and continuity of stress and displacement interpolation functions are very important in a mixed formulation, as certain choices might lead to meaningless results (Zienkiewicz and Taylor 1989). For stability of the formulation the rank of matrix \mathbf{T} in the expression $\mathbf{T}^T(\mathbf{F}_s^{-1})^{-1}\mathbf{T}$ should not be larger than the rank of the flexibility matrix. For this to be the case the number of unknowns n'_d in vector \mathbf{u} after excluding the rigid body modes should be less or equal to the number of unknowns n_s in vector $\boldsymbol{\sigma}$

$$n_s \geq n'_d \quad (39)$$

The condition in (39) is necessary but not sufficient to ensure convergence of an element. Numerical difficulties may arise due to excessive continuity requirements, as it becomes apparent with an element that is subjected to a concentrated force at an intermediate node. While the exact solution shows a stress jump at the point of load application, treating the steel stresses as independent degrees of freedom results in a continuous stress field. This, in turn, might lead to oscillations of the displacement increments. To overcome this problem Zienkiewicz and Taylor (1989) recommend that stress continuity be relaxed locally, thus, leading to the decision in this paper to condense out the stress degrees of freedom according to (35)–(37).

The selection of suitable stress and displacement interpolation functions is further guided by de Veubeke's principle of limitation (1965): there is no accuracy gain by increasing the order of the stress field beyond the order of the strain field that respects the strain-displacement compatibility condition. This is, however, relevant only under linear elastic material behavior and advantages might accrue from higher order stress interpolation functions when the material behaves nonlinearly. The potential advantages from higher order stress interpolation functions are not pursued further in this paper.

The simplest choice within the constraints of de Veubeke's principle is a constant stress field with a linear displacement field. This choice, however, does not allow for stress redistribution in the element in the nonlinear range; in fact, this case is identical to the displacement formulation with a linear displacement interpolation, since it produces the same stress variation for linear and nonlinear material behavior. An improvement over the displacement formulation is, therefore, only possible with a mixed formulation that uses a quadratic displacement interpolation function and a linear steel stress interpolation function. This improvement only manifests itself in the nonlinear range of material behavior, as the mixed model accommodates stress redistribution and strain localization in elements of large size. By contrast, under linear elastic conditions this formulation is identical to a displacement model with quadratic interpolation functions. A mixed formulation with higher than quadratic displacement interpolation functions and corresponding orders of stress interpolation

functions is also possible, but clearly computationally more demanding and is not pursued further in this study.

In the following correlation studies the mixed formulation is implemented with quadratic displacement interpolation and linear stress interpolation functions. The middle displacement degree of freedom and the end stress degrees of freedom are condensed out in the numerical implementation, so that only the end node displacements remain according to (37).

EVALUATION OF MODELS BY CORRELATION WITH EXPERIMENTS AND BY NUMERICAL STUDIES

The different models of the anchored reinforcing bar are compared by correlation studies with the monotonic response of an anchored reinforcing bar tested by Viwathanatepa et al. 1979. The reinforcing bar is a straight No. 8 (25 mm diameter) reinforcing bar that is embedded in a well-confined concrete block with an anchorage length of 25 bar diameters. Two specimens were tested: one under monotonic pull-out loading at one end with no stress at the other and the second with monotonic pull-out and simultaneous push-in with equal end steel stress at the other end. These specimens have been extensively used in previous correlation studies and the experimental response is very well documented. The analytical studies make use of the nonlinear steel stress-strain relation by Menegotto and Pinto (Filippou et al. 1983a). The modulus of elasticity of the bar is 205 GPa, the yield strength is 470 MPa, and the strain hardening ratio is 1.4%. The bond stress-slip relation follows the model by Eligehausen et al. (1983). The material parameters of the bond model for the confined anchorage zone region and the unconfined cover region used in the study are summarized in Fig. 2. The unconfined cover zone where a pull-out cone has been observed to form in experiments is assumed to extend for a length equal to four bar diameters at both ends of the anchored bar.

A displacement model with quadratic displacement interpolation functions and a fine mesh discretization with 42 elements is used as numerical benchmark. These results are compared with three models using only six equally spaced elements: (1) a displacement model with quadratic displacement interpolation; (2) the flexibility model by Monti et al. (1993, 1997); and (3) the proposed two field mixed model with stress condensation. Five Gauss-Lobatto integration points are used in the numerical evaluation of the integrals. In this integration scheme two control points are located at the element ends and the remaining three inside the element. This fact plays a role in the observed field discontinuities of the various

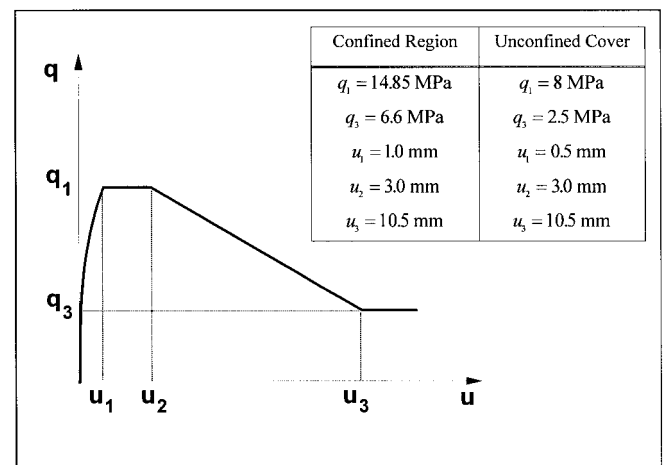


FIG. 2. Material Parameters of Bond Model for Monotonic Tests (1 MPa = 145 psi, 1 mm = 0.0394 in.)

methods, which would be less evident if only integration points inside the elements were used, as is the case with the classical Gauss integration.

The global end force-displacement response for the flexibility and mixed model under monotonic pull-out are compared with the experiment and the benchmark case in Fig. 3. Excellent agreement of all models with experimental results is observed, with the mixed formulation giving virtually identical results with the benchmark model.

Figs. 4 and 5 compare the strain and stress distribution for a displacement model with a coarse mesh of six equally spaced elements with the benchmark case. These distributions are de-

scribed for four load stages: a load in the elastic range at incipient yielding of the bar (A), a load shortly after steel yielding (B), a load after some yield penetration (C), and a load for a significant yield penetration (D). These load stages are also identified on the load-displacement response in Fig. 3. While there are no significant differences between the two cases in the linear elastic range, the displacement model with the coarse mesh fails to capture the strain localization at the tip of the bar. Thus, the end strain value deviates significantly from the benchmark solution. This leads to significant deviations of the steel stress field for the coarse mesh from the benchmark case in Fig. 5 with very pronounced steel stress discontinuities at the element boundary for the coarse mesh. Under large inelastic strains and cyclic loading conditions, such discontinuities are known to cause spurious unloading of portions of the bar and may result in lack of convergence of the solution algorithm. Similar but less pronounced discrepancies between the displacement model with coarse mesh and the benchmark case are also evident in the bond stress distributions in Fig. 6, while the relative dip distribution in Fig. 7 shows good agreement between the two mesh configurations. From this correlation it is obvious that displacement models require a rather fine mesh discretization to produce satisfactory results. Even with a fine discretization Fig. 5 shows that noticeable stress discontinuities appear at element boundaries.

Figs. 8–11 compare the distributions of steel strain and stress, bond stress, and relative slip for the flexibility and two-field mixed models with those of the benchmark displacement model. The flexibility and two-field mixed models use the coarse mesh of six equally spaced elements. Even with this

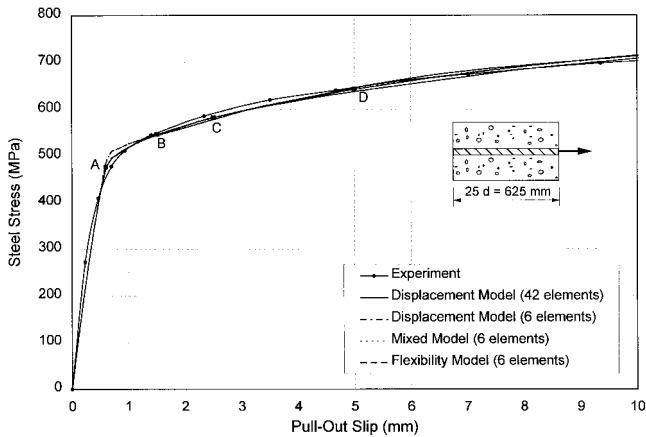


FIG. 3. Global Response for Monotonic Pull Case

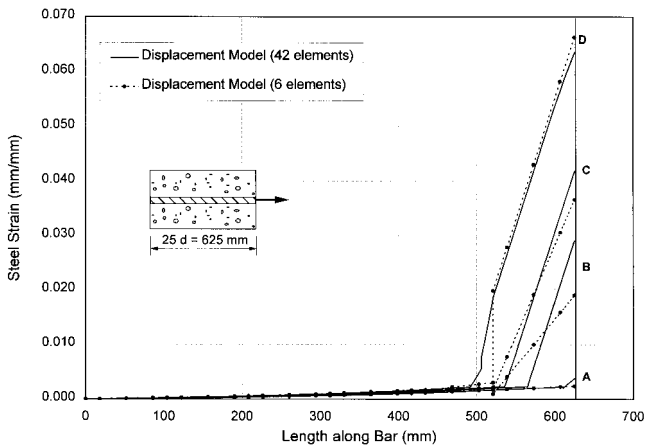


FIG. 4. Strain Distribution for Monotonic Pull Case (Displacement Model)

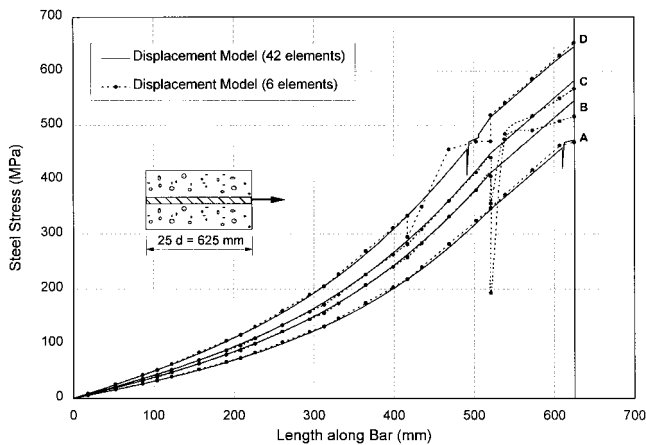


FIG. 5. Stress Distribution for Monotonic Pull Case (Displacement Model)

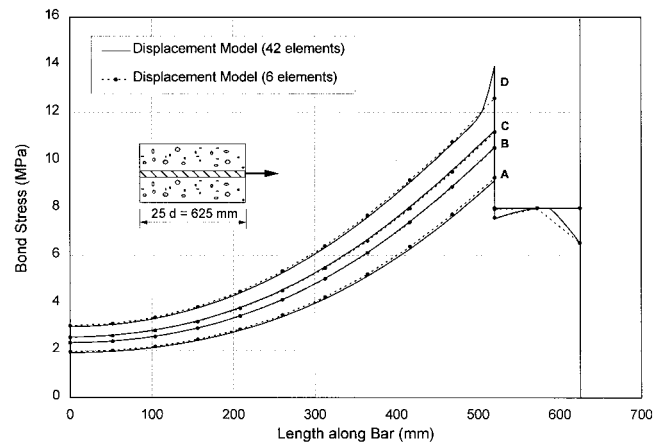


FIG. 6. Bond Distribution for Monotonic Pull Case (Displacement Model)

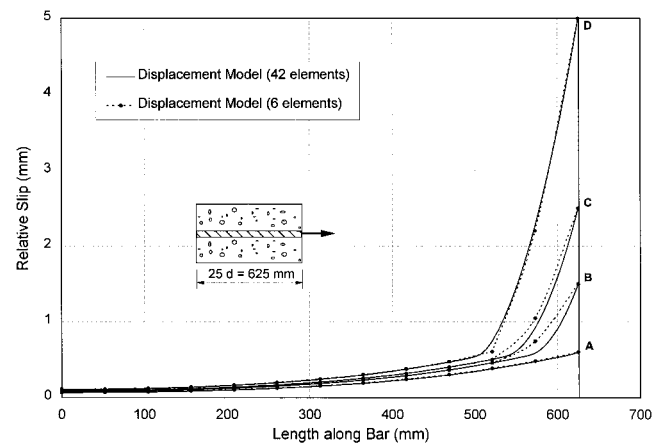


FIG. 7. Relative Slip Distribution for Monotonic Pull Case (Displacement Model)

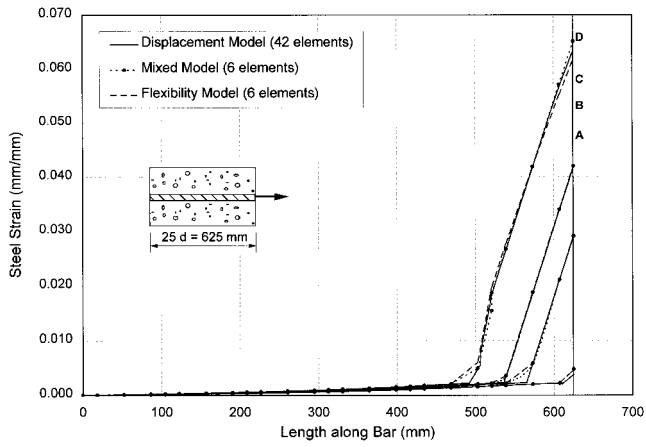


FIG. 8. Strain Distribution for Monotonic Pull Case

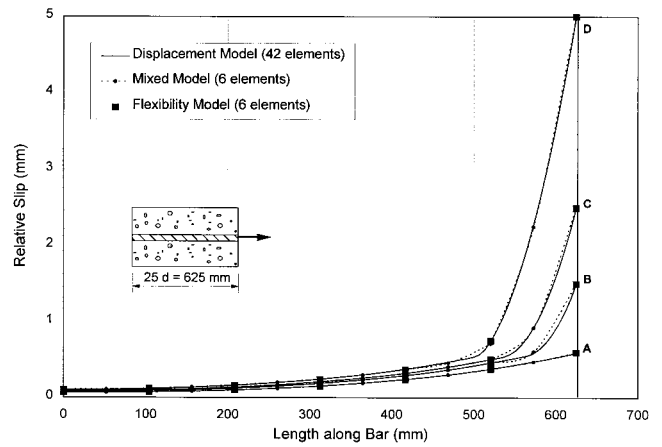


FIG. 11. Relative Slip Distribution for Monotonic Pull Case

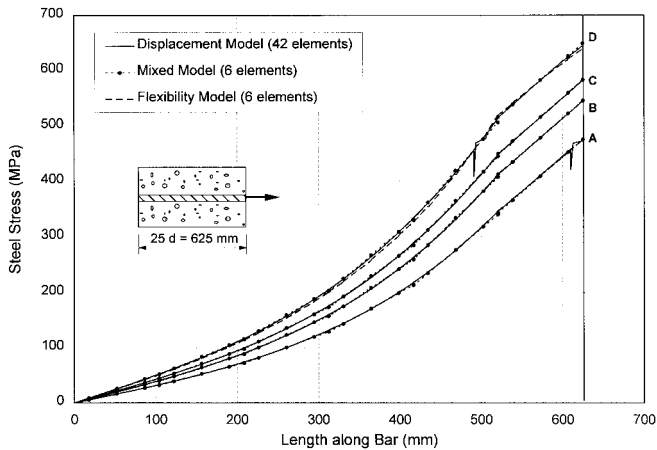


FIG. 9. Stress Distribution for Monotonic Pull Case

by increasing the number of sampling points of the slip interpolation. It is worth noting that the steel stress discontinuities at the element boundaries are negligibly small for the mixed formulation in Fig. 9, as identified by the round black markers. In spite of significant slip at the yielding end of the anchored reinforcing bar, the other end does not experience large strains and a complete pull-out of the bar is not possible for the anchorage length of 25 bar diameters, even though bond damage is significant along the yielding portion of the bar, as is evident in the bond stress distribution in Fig. 10. Thus, the end force-displacement response does not exhibit any strength loss in Fig. 3. To examine a case with global softening, the second specimen is used. In this case the bar is pulled at one end and

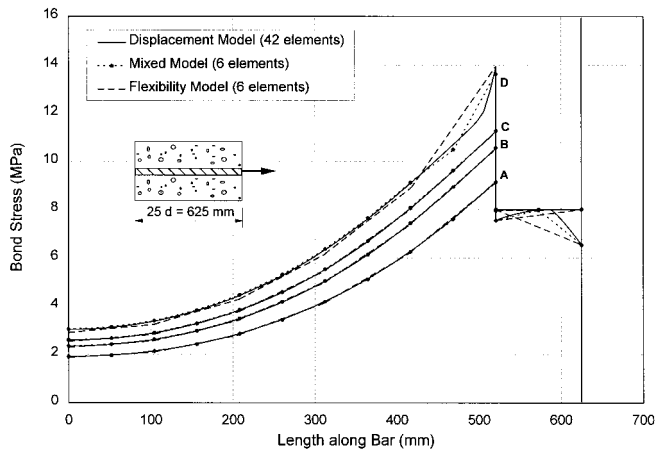


FIG. 10. Bond Distribution for Monotonic Pull Case

coarse mesh, the distributions for these models agree extremely well with the displacement solution using a fine mesh. The only obvious advantage of the two-field mixed model over the flexibility model is its superior performance regarding the slip and bond distribution. The flexibility model satisfies the bond-slip relation only at the ends of the element; the element is, thus, incapable of supplying any slip distribution inside the element in Fig. 11 and the linear bond stress distribution is simply based on the bond stress values at the element ends. This fact limits the maximum size of element that can be used for reasonable accuracy in the bond stress and relative slip approximation. By contrast, the mixed model does not have any such limitation and the element accuracy can be increased

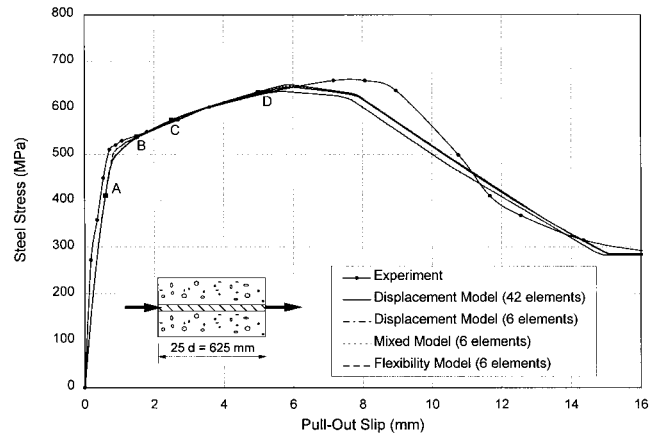


FIG. 12. Global Response for Monotonic Pull-Push Case

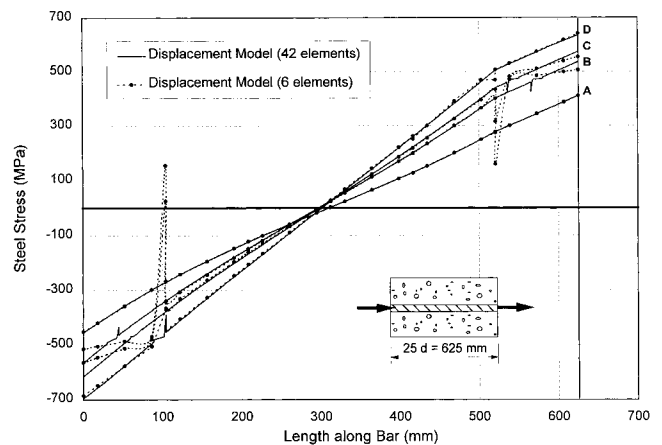


FIG. 13. Stress Distribution for Monotonic Pull-Push Case (Displacement Model)

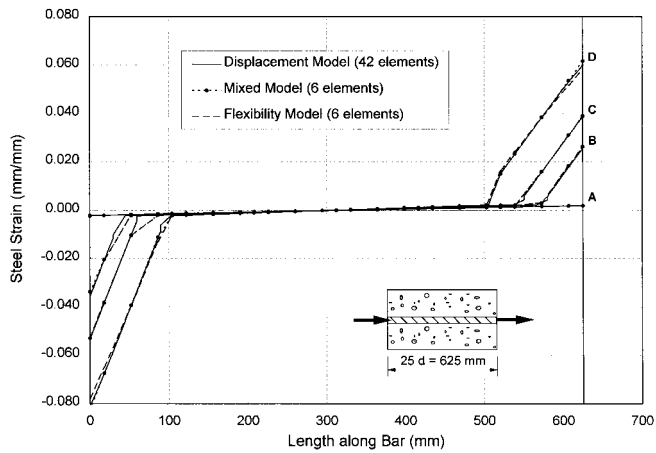


FIG. 14. Strain Distribution for Monotonic Pull-Push Case

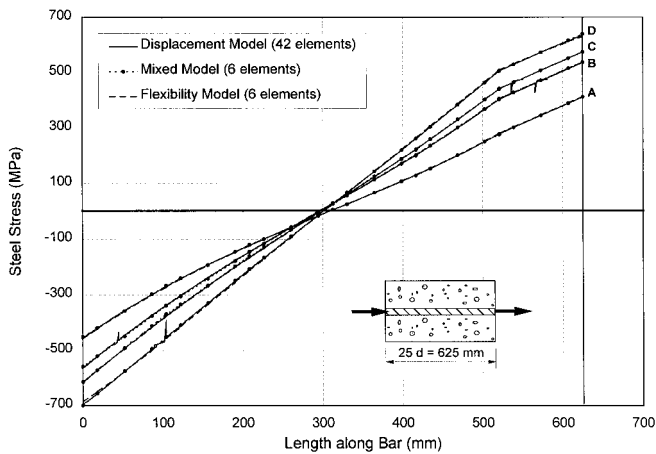


FIG. 15. Stress Distribution for Monotonic Pull-Push Case

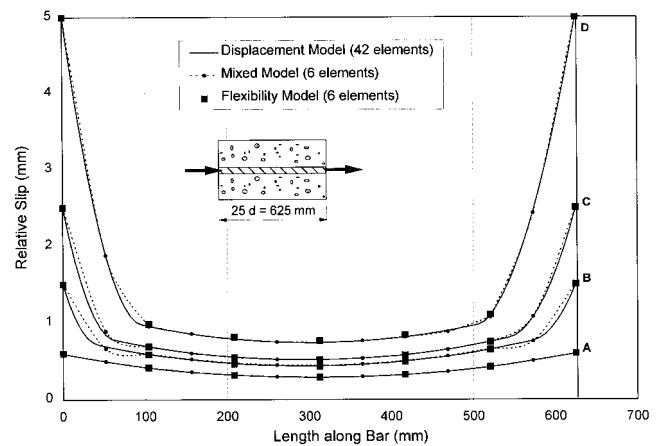


FIG. 16. Relative Slip Distribution for Monotonic Pull-Push Case

pushed at the other. Thus, the stress transfer requirements are more severe and bond is eventually damaged along the entire bar, leading to pull-through and strength loss. The end force-displacement response of this case is shown in Fig. 12, where very good agreement of all models with the experiment is observed. The response of the displacement model with a coarse and fine mesh is compared in Fig. 13, which shows again notable stress discontinuities at the element boundaries near the yield front at both ends of the anchored bar. Figs. 14–17 compare the response of the benchmark displacement case with that of the flexibility and mixed model. The excellent agreement of the steel strain and stress distributions of the

flexibility and mixed model with the displacement model having seven times as many elements in Figs. 14 and 15 is impressive. Fig. 16 shows the inability of the flexibility model to represent the slip distribution inside the element and markers are used to identify the slip values at the element ends. Near the yielding ends of the anchored bar this results in stronger discrepancies of the bond stress distribution of the flexibility model from the benchmark case than is the case for the mixed model (Fig. 17).

In order to test the numerical performance of the proposed mixed model under large slip reversals, the analytical results are compared with experimental data in Fig. 18. The test is described in Viathanatepa et al. (1979), and the material pa-

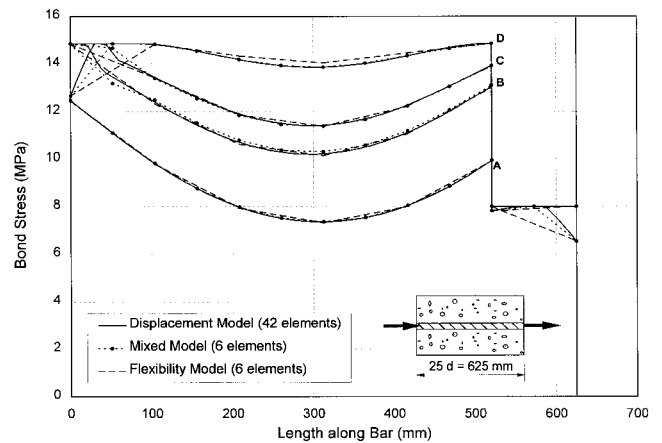


FIG. 17. Bond Distribution for Monotonic Pull-Push Case

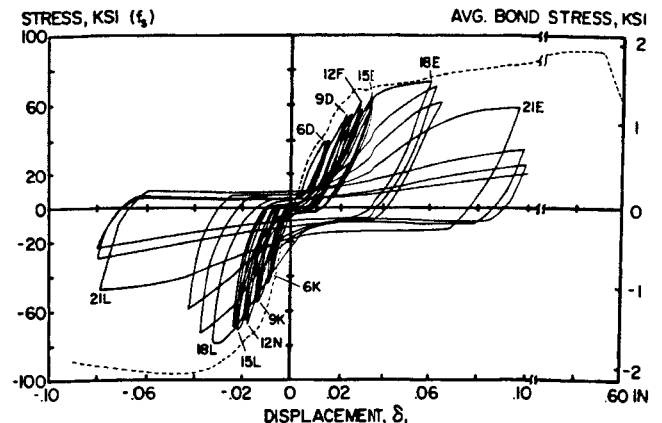


FIG. 18(a). Experimental Stress Slip Response under Pull-Push Slip Reversals

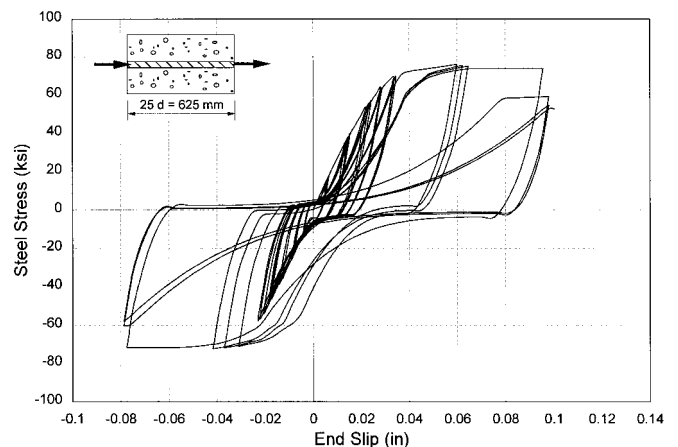


FIG. 18(b). Analytical Stress Slip Response under Pull-Push Slip Reversals

rameters are the same as for the preceding monotonic studies. The mixed formulation shows very robust numerical behavior and is able to represent accurately the loss of strength and stiffness of the anchored bar under large slip reversals.

SUMMARY AND CONCLUSIONS

This paper compares different analytical models for an anchored reinforcing bar: the well-established displacement formulation, a recently proposed flexibility model, and a new two-field mixed formulation. In the new model independent interpolation functions are used for the steel stress and the relative slip. The selection of the order and continuity requirements for the interpolation functions is discussed.

The flexibility model and the mixed model are able to match the accuracy of the displacement model using a much coarser finite element mesh. On account of the resulting reduction in the number of global degrees of freedom, they are computationally more efficient than the displacement model, even though the element state determination involves several extra steps. Moreover, they are characterized by robust numerical behavior even in the presence of strain softening, when the displacement model is plagued by numerical instabilities that result from the weighted average satisfaction of element equilibrium and the resulting stress discontinuities at element boundaries. Even though the stress continuity is relaxed for the mixed model with stress condensation, equilibrium is satisfied in a strict sense and this leads to superior behavior under large slip reversals. The proposed mixed model is also superior to a recently proposed flexibility model, because it interpolates the slip within the element, thus permitting the accurate description of relative slip and bond stress distributions, even for elements of large size. Moreover, in contrast to the flexibility model, the proposed mixed formulation results in a symmetric stiffness matrix and is characterized by faster numerical convergence due to the consistent approximation of the bond slip response within the element. This good numerical performance has been verified by simulation studies of anchored reinforcing bar models under large monotonic and cyclic end displacements with discretizations using large finite elements.

ACKNOWLEDGMENTS

The writers wish to thank Prof. Robert L. Taylor for discussions and suggestions regarding the formulation and numerical implementation of the mixed formulation in program FEAP. Partial support for this project was provided by the California Department of Transportation under Grant Contract RTA-59A131. This support is gratefully acknowledged. The opinions expressed in the paper are those of the writers and do not reflect the views of the sponsoring agency.

APPENDIX I. REFERENCES

- ASCE Task Committee on Finite Element Analysis of Reinforced Concrete Structures. (1982). *Finite element analysis of reinforced concrete structures*. ASCE, Reston, Va.
- Bertero, V. V., Popov, E. P., and Viwathanatepa, S. (1978). "Bond of reinforcing steel: Experiments and a mechanical model." *Proc., IASS Symp. on Nonlinear Behavior of Reinforced Concrete Spatial Struct.*, 3-17.
- Ciampi, V., and Carlesimo, L. (1986). "A nonlinear beam element for seismic analysis of structures." *Proc., 8th Eur. Conf. on Earthquake Engng.*, 6.3/73-6.3/80.
- Ciampi, V., Eligehausen, R., Bertero, V. V., and Popov, E. P. (1982). "Analytical model for concrete anchorages of reinforcing bars under generalized excitations." *UCB/EERC-82/83*, Earthquake Engrg. Res. Ctr., University of California, Berkeley.
- de Groot, A. K., Kusters, G. M. A., and Monnier, T. (1981). "Numerical modeling of bond-slip behavior." *Heron, Concrete Mech.*, Netherlands, 26(1B).

- Eligehausen, R., Popov, E. P., and Bertero, V. V. (1983). "Local bond stress-slip relationships of deformed bars under generalized excitations." *UCB/EERC-83/23*, Earthquake Engrg. Res. Ctr., University of California, Berkeley.
- Filippou, F. C. (1986). "A simple model for reinforcing bar anchorages under cyclic excitations." *J. Struct. Engrg.*, ASCE, 112(7), 1639-1659.
- Filippou, F. C., Popov, E. P., and Bertero, V. V. (1983a). "Effects of bond deterioration on hysteretic behavior of reinforced concrete joints." *UCB/EERC-83/19*, Earthquake Engrg. Res. Ctr., University of California, Berkeley.
- Filippou, F. C., Popov, E. P., and Bertero, V. V. (1983b). "Modeling of reinforced concrete joints under cyclic excitations." *J. Struct. Engrg.*, ASCE, 109(11), 2666-2684.
- Keuser, M., and Mehlhorn, G. (1987). "Finite element models for bond problems." *J. Struct. Engrg.*, ASCE, 113(10), 2160-2173.
- Monti, G., Filippou, F. C., and Spacone, E. (1997). "A finite element for anchored bars under cyclic load reversals." *J. Struct. Engrg.*, ASCE, 123(5), 614-623.
- Monti, G., Spacone, E., and Filippou, F. C. (1993). "Model for anchored reinforcing bars under seismic excitations." *Rep. EERC 93-08*, Earthquake Engrg. Res. Ctr., University of California, Berkeley.
- Neuenhofer, A., and Filippou, F. C. (1997). "Evaluation of nonlinear frame finite element models." *J. Struct. Engrg.*, ASCE, 123(7), 958-966.
- Ngo, D., and Scordelis, A. C. (1967). "Finite element analysis of reinforced concrete beams." *ACI J.*, 64(3), 152-163.
- Nilson, A. H. (1971). "Internal measurements of bond slip." *ACI J.*, 69(7), 439-441.
- Tassios, T. P., and Yannopoulos, P. J. (1981). "Analytical studies on reinforced concrete members under cyclic loading based on bond stress slip relations." *ACI J.*, 78(3), 206-216.
- Viwathanatepa, S., Popov, E. P., and Bertero, V. V. (1979). "Effects of generalized loadings on bond of reinforcing bars embedded in confined concrete blocks." *UCB/EERC-79/22*, Earthquake Engrg. Res. Ctr., University of California, Berkeley.
- Yankelevsky, D. Z. (1985). "New finite element for bond-slip analysis." *J. Struct. Engrg.*, ASCE, 111(7), 1533-1542.
- Zienkiewicz, O. C., and Taylor, R. L. (1989). *The finite element method*. Vol. 1, *Basic formulation and linear problems*. McGraw-Hill, London.
- Zulfiqar, N., and Filippou, F. C. (1990). "Model of critical regions in reinforced concrete frames under earthquake excitations." *UCB/EERC-90/06*, Earthquake Engrg. Res. Ctr., University of California, Berkeley.

APPENDIX II. NOTATION

The following symbols are used in this paper:

- $\mathbf{a}(x)$ = vector of displacement shape functions;
 $\mathbf{b}(x)$ = vector of stress interpolation functions;
 $\mathbf{b}_b(x)$ = vector of bond interpolation functions;
 \mathbf{F}_s = steel element flexibility matrix;
 \mathbf{K}_b = bond contribution to element stiffness matrix;
 \mathbf{K}_s = steel contribution to element stiffness matrix;
 $k_b(x)$ = bond stiffness at x ;
 $k_s(x)$ = steel stiffness at x ;
 n_a, n_s = order of displacement and stress interpolation functions;
 \mathbf{P} = applied load vector;
 \mathbf{Q}_b = bond contribution resisting load vector;
 \mathbf{Q}_s = steel contribution to resisting load vector;
 $q(x)$ = bond stress at x ;
 \mathbf{q} = vector of element bond stresses;
 \mathbf{u} = vector of element displacements;
 $u(x)$ = relative slip at x ;
 $u_s(x), u_c(x)$ = steel and concrete axial displacement at x , respectively;
 \mathbf{u}_r = vector of element displacement residuals;
 Δ = increment of;
 δ = virtual field;
 $\epsilon(x)$ = steel strain at x ;
 ρ = ratio of reinforcing bar perimeter to bar area;
 $\sigma(x)$ = steel stress at x ; and
 $\boldsymbol{\sigma}$ = vector of element steel stresses.